Quaternary Research (2025), 1–11
doi:10.1017/qua.2025.10049

Research Article

A new relative sea-level curve from Inglefield Land, northwest Greenland

Karlee K. Prince and Jason P. Briner
Department of Earth Sciences, University at Buffalo, Buffalo, NY, USA

Abstract

We report a new relative sea level curve from Inglefield Land, northwest Greenland, to investigate the transition from maximum to minimum loading across Nares Strait. We sampled marine bivalves and terrestrial macrofossils for radiocarbon dating from raised marine terraces in Rensselaer Valley, Inglefield Land (78.58°N, 70.71°W) to constrain relative sea level through the Holocene. The oldest terrestrial macrofossil of 9010–8650 cal yr BP provides a minimum-limiting constraint for the deglaciation. Sea level fell rapidly from the marine limit at 85 ± 4 m to 37.5 ± 4 m above sea level (m asl) between 9010–8650 and 7970–7790 cal yr BP at a rate of 49 m/ka. The rate of sea -level fall decreased to 11 m/ka between 7970–7790 and 5320–5060 cal yr BP, when it fell from 37.5 ± 4 to 9 ± 4 m asl. After 5,320–5,060 cal yr BP, we estimate sea level fell at a lower rate of 2 m/ka to modern sea level. The period of fastest emergence in Inglefield Land is earlier in time than in Hall Land, reflecting earlier deglaciation, and is steeper than in Hall Land and Washington Land. This sea-level history captures the transition from the style of emergence from Pituffik to Hall Land.

Keywords: Relative sea level; Greenland Ice Sheet; Glacial isostatic adjustment; Nares Strait; Radiocarbon dating

Introduction

Land-based ice is melting and raising global sea levels (Edwards et al., 2021), and the Greenland Ice Sheet is one of the leading contributors to global sea-level rise (IPCC, 2019). The amount of sea-level rise from future retreat of the Greenland Ice Sheet is predicted from ice sheet models that consider different future warming scenarios (Goelzer et al., 2020). To increase confidence in sea-level rise estimates, it is useful to compare ice sheet model output with geologic constraints of past ice sheet changes (Briner et al., 2020). The Mid-Holocene (~9–5 ka) is a geologically recent warm period often targeted to gauge ice sheet response to past warming because it is a partial analog for future warming (Axford et al., 2021). Data-model comparisons during this time are difficult, because the ice sheet was smaller than at present in most areas between 6.5 ka and the Little Ice Age (1400–1850 CE) (Leger et al., 2024). Reconstructions of relative sea level can track glacial isostatic adjustment through the entire Holocene, allowing for insights into glacial activity from 6.5 ka to the Little Ice Age (Antwerpen et al., 2024). These reconstructions can be directly compared with ice sheet model output to assess model fit or guide adjustments to learn about the ice-sheet history (Gowan, 2023). As there is spatial heterogeneity in glacial isostatic uplift patterns around Greenland, a dense network of sites is increasingly important to understand ice-sheet history (Long et al., 2011).

Nares Strait is an area with spatial heterogeneity in the uplift pattern in part due to the convergence of the Greenland and Innuitian Ice Sheets. Here the marine limit varies along the axis of Nares Strait in a bullseye fashion (Long et al., 2011), which is a pattern that is reproduced in glacial isostatic adjustment models (Lecavalier et al., 2014, 2017). Despite the complicated pattern shown by the marine limit variability and glacial isostatic adjustment model output, the relative sea-level data are mostly limiting data: radiocarbon ages that require sea level to be at an unspecified height above the elevation of the sample (England, 1985; Fredskild, 1985; Funder, 1990; Kelly and Bennike, 1992; Bennike, 2002; Figs. 1 and 2). Elsewhere, data are considered sea level index points (SLIPs), which are typically radiocarbon ages that tie a specific elevation of a paleo–sea level height to a given time; SLIPs are typically derived from dated marine shells in marine deltas or terraces (Hall et al., 2010) or from isolation basin studies (e.g., Long et al., 2011). Because this region has a gradient in sea-level history from SW to NE, and potentially an even more complicated sea level than the bullseye pattern, a SLIP-based study in the middle of Nares Strait helps the spatial distribution of sea-level data in the region and allows for a tighter window for models to target.

Glueder et al. (2022) recently produced a relative sea level reconstruction using marine bivalves from raised marine deposits with a novel $\delta^{18}O$-based habitat depth relationship in Hall Land and Washington Land (Figs. 1 and 2). Using their relative sea level reconstruction, Glueder et al. (2022) tested ice-history scenarios and interpreted a Middle Holocene sea-level standstill being caused by hundreds of meters of ice-cap growth from 6 to 2 ka, followed by sea-level fall from 2 ka to the present due to subsequent

Corresponding author: Karlee K. Prince; Email: karleepr@buffalo.edu
Cite this article: Prince, K.K., Briner, J.P., 2025. A new relative sea-level curve from Inglefield Land, northwest Greenland. *Quaternary Research*, 1–11. https://doi.org/10.1017/qua.2025.10049

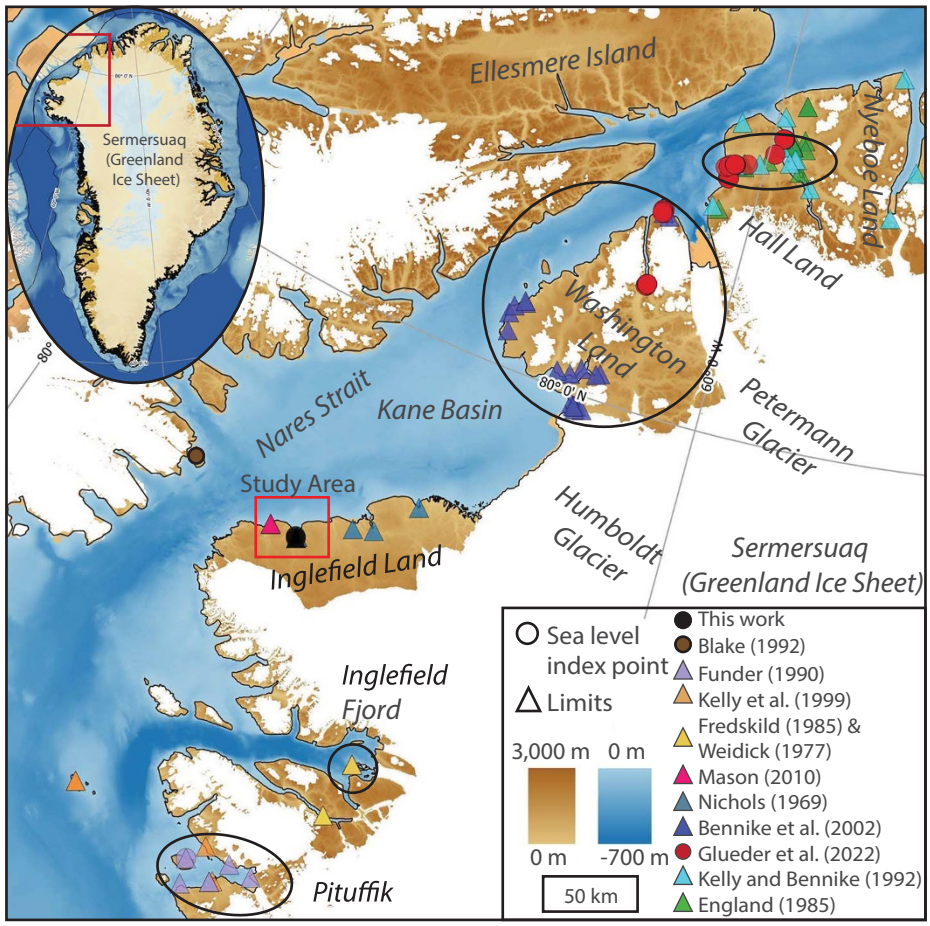

Figure 1. Northwest Greenland and Nares Strait. Individual sea level index points (SLIPs) are plotted as circles, and individual sea-level limits are plotted as triangles. Each study is assigned a different color. Large circles are groups of sea-level data that are plotted together in Figures 2, 5, and 6. The inset map shows the study area box in Greenland. The Greenland Ice Sheet, land elevation, and ocean bathymetry are from BedMachine v. 4 (Morlighem et al., 2017, 2021). Modern ice that is separate from the Greenland Ice Sheet is shown with the Randolph Glacier Inventory (RGI Consortium, 2023). Data are from Blake (1992), Funder (1990), Kelly et al. (1999), Fredskild (1985), Weidick (1977), Mason (2010), Nicholas (1969), Bennike et al. (2002), Glueder et al. (2022), Kelly and Bennike (1992), and England (1985).

ice-cap disappearance. This inferred ice-cap history challenges field data from the nearby Petermann and Humbolt Glaciers that were advancing through the Neoglacial and Little Ice Age, reaching near the present margin at least 2.8 ± 0.3 ka and followed by a regionally maximum Late Holocene extent ~300 ± 200 years ago (Reusche et al., 2018). Additionally, the coolest part of the Holocene following the thermal maximum is recorded in the last millennium in lake records from Pituffik to Inglefield Land (Blake et al., 1992; Briner et al., 2016; Lasher et al., 2017; Axford et al., 2019). This pattern of decreasing temperature through the Middle and Late Holocene and into the Little Ice Age is found in all sectors of Greenland (Kjær et al., 2022). Additional SLIPs from this region could help clarify the Holocene sea level and ice-loading history in northwestern Greenland.

We present a new relative sea level curve based on SLIPs and limiting data from a flight of raised marine terraces on Inglefield Land, northwest Greenland, to fill a spatial data gap and help understand the history of ice loading. We find that the Inglefield Land coastline deglaciated before 9010–8650 cal yr BP, and the land emerged at a rate of 49 m/ka between 9010–8650 and 7970–7790 cal yr BP. After 7970–7790 cal yr BP, emergence slowed to 11 m/ka until ~5000, whereupon sea level likely then fell continuously to the present.

Study area

In northwest Greenland, the Greenland and Innuitian Ice Sheets converged in Nares Strait during the last glacial maximum, flowing southward into Baffin Bay and northward into the Arctic Ocean (England, 1999; Couette et al., 2022; Batchelor et al., 2024). The oldest marine bivalves are 10,700–9720 and 10,370–9440 cal yr BP from Pituffik and Hall Land, respectively, and 7920–7450 cal yr BP from southwest Washington Land (England, 1985; Kelly et al., 1999; Bennike, 2002; see Fig. 1 for locations). The marine limit increases from 40 m above sea level (m asl) near Pituffik to 124 m asl in Hall Land (Nichols, 1969; Kelly and Bennike, 1992; Bennike, 2002; Fig. 2). In Hall Land and Washington Land, the land emergence was slow in the beginning, rapid in the Mid-Holocene, and slowed to the present (England, 1985; Kelly and Bennike, 1992; Bennike, 2002). In Inglefield Fjord and Pituffik, land emergence was rapid before slowing to the present, although there are fewer data to constrain this pattern (Fredskild, 1985; Funder, 1990; Kelly et al., 1999). These patterns together likely reflect the "unzipping" of the two coalesced ice sheets (England, 1999).

The glacial history of Inglefield Land is well known from sediment cores, radiocarbon dating of reworked marine bivalves, and cosmogenic nuclide exposure dating. Sediment cores from

https://doi.org/10.1017/qua.2025.10049 Published online by Cambridge University Press

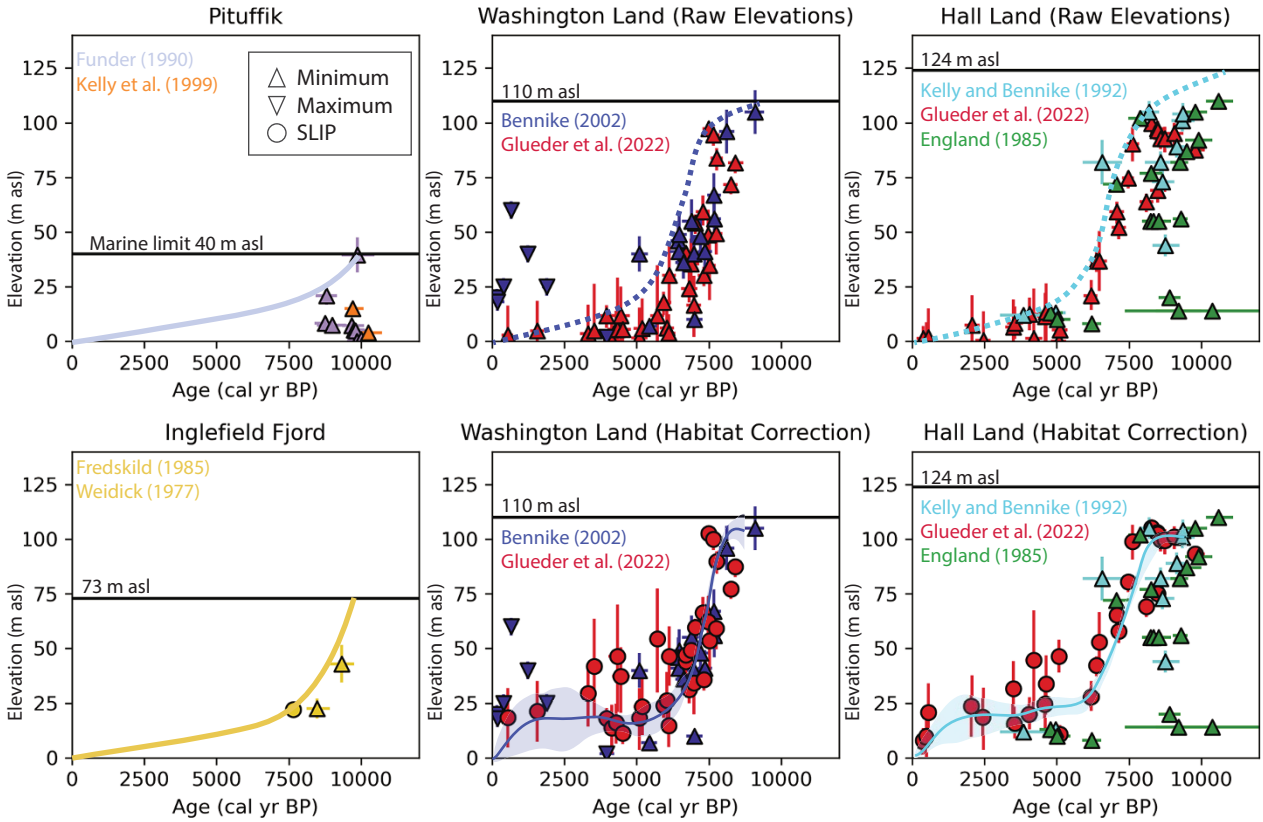

Figure 2. Regional sea-level data with estimated sea-level histories shown as solid and dashed lines. As in Figure 1, sea level index points (SLIPs) are circles, and sea-level limits are triangles. They are color coded by publication, as listed in the panels: Weidick (1977); England (1985); Fredskild (1985); Funder (1990); Kelly and Bennike (1992); Bennike (2002); and Glueder et al. (2022). Our study site lies between Inglefield Fjord and Washington Land. The marine limit is plotted as a solid black line with the elevation labeled above it. Washington and Hall Land have two plots each. The plots labeled "Raw Elevations" have Glueder et al. (2022) samples as minimum limits, and they are plotted as red triangles with their raw elevations (using collection elevation instead of adjusted elevation). The plots labeled "Habitat Correction" have Glueder et al. (2022) samples as SLIPs as red circles and are plotted with their habitat-corrected depths. Glueder et al. (2022) habitat-corrected model output shown with uncertainty.

Kane Basin, offshore of Inglefield Land, record deglaciation before 9000–8300 cal yr BP (Georgiadis et al., 2018). Nichols (1969) described the geomorphology of Inglefield Land and investigated both the raised beach deposits adjacent to our study area in Rensselaer Bay and the raised marine deltas across the river from our study site; a radiocarbon date on peat constrains deglaciation of the coastline in Rensselaer Bay to before 9130–8180 cal yr BP. Søndergaard et al. (2020) used cosmogenic nuclide exposure dating and radiocarbon dating of reworked marine bivalves to show the ice sheet reached its present margin by 6.7 ± 0.3 ka and was smaller than present from sometime before 5930–5750 to 600–500 cal yr BP. Mason (2010) investigated a suite of raised beaches at Cape Grinnell (~20 km northeast of our study site) and inferred sea level fell rapidly at Cape Grinnell from the 72 m asl marine limit to approximately 20 m asl, when a short standstill occurred, followed by a fall to around 5 m, where he inferred a transgression occurred, before sea level fell to the present. Mason (2010) added age control to his work with radiocarbon ages from marine bivalves reworked in solifluction lobes and from within beach ridges (minimum ages) and ages on caribou and muskox bone from Thule settlement remains that constrain sea level to a lower elevation (maximum ages). Finally, a well-constrained relative sea level curve from Cape Hershel, Ellesmere Island, 90 km due west and across Nares Strait from our study site, shows rapid sea-level fall along the Ellesmere Island coast after deglaciation at 8300–9000 cal yr BP and a steady fall to the present (Blake, 1992).

Methods

We investigated six raised marine terraces along the west side of the Rensselaer River. These terraces formed when delta deposition ended as glacial isostatic adjustment uplifted the delta above the ocean surface, and the river eroded through the paleo-delta deposit to the new base level (Fig. 3). We measured the elevation of terrace surfaces and targeted sediment exposures that contained material for radiocarbon dating (Fig. 4). Radiocarbon ages on plant and marine bivalve samples are used to determine the timing of delta progradation and define the timing of sea level at the elevation of the topset/foreset contact.

Table 1 reports the terrace surface elevation estimations and the relationship between the radiocarbon sample locations and past sea level. In the field, we determined the elevation of terraces surface using a handheld GPS. Similar to our handheld GPS, ArcticDEM reports elevation in meters above the WGS 84 ellipsoid with a ±4 m uncertainty across the entire product (Porter et al., 2023). We use the ArcticDEM to reduce uncertainties. We averaged five elevation points on each terrace spaced out along the northern end of the terrace, which was the seaward-facing end. On average, the reported present sea surface height above the ellipsoid in this area is 11 ± 0.1 m. We subtract this from the terrace and sample elevation to report terrace elevation in meters above sea level (m asl).

In the University at Buffalo Glacial History Laboratory, we rinsed marine bivalve shells with deionized water to remove

https://doi.org/10.1017/qua.2025.10049 Published online by Cambridge University Press

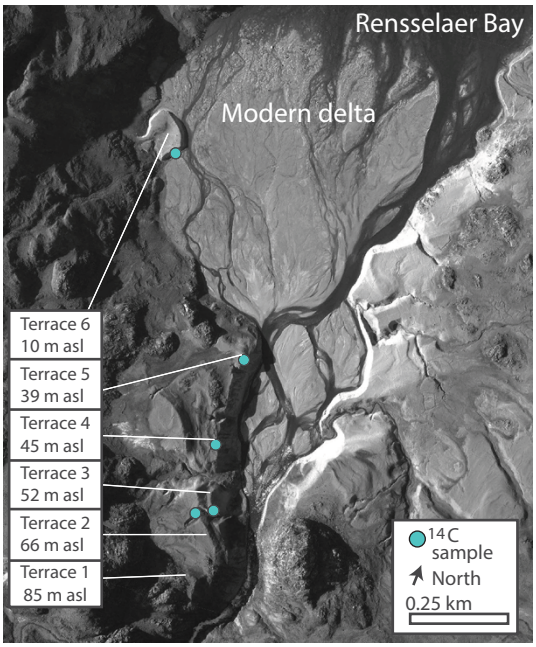

Figure 3. Polar Geospatial Center 0.5 m imagery of Rensselaer Bay. Raised terraces along the west side of the river are labeled, and blue circles indicate radiocarbon samples. Imagery © 2021 Maxar.

sediment, scraped away friable outer layers of the shells with forceps, and freeze-dried them. For radiocarbon dating, we targeted the shell umbo, because it is the thickest part of the shell and harder to contaminate than the thin edges (e.g., Hall et al., 2010). We rinsed terrestrial macrofossils with deionized water then freeze-dried single *Calligeron* sp. moss strands and a *Salix* sp. stem. We sent samples to the National Ocean Sciences Accelerated Mass Spectrometry (NOSAMS) Laboratory for radiocarbon dating. NOSAMS performed acid-base-acid (ABA) pretreatments before converting samples to graphite and running them on the accelerated mass spectrometer (Vogel et al., 1984; Pearson et al., 1997; Shah Walter et al., 2015; Elder et al., 2019). The $\delta^{13}C$ was measured on an isotope-ratio mass spectrometer using the CO_2 from each sample; uncertainties are <0.1‰, and we report $\delta^{13}C$ values as ‰ VPDB.

Table 2 reports radiocarbon data and ages; in the text we report the maximum and minimum of the 2-sigma age range. We used Calib8.1 with the IntCal20 dataset to calibrate terrestrial samples (Stuiver and Reimer, 1993; Reimer et al., 2020). We radiocarbon dated marine bivalves from five of the six terraces, and terrestrial and marine sample pairs from three of the six terraces. We used the online DeltaR application (http://calib.org/deltar) to calculate the ΔR for these sample pairs (Reimer and Reimer, 2017). This technique uses the calibrated age of the terrestrial sample to predict a contemporaneous uncalibrated marine age—the difference between this prediction and the measured uncalibrated marine ^{14}C age is the ΔR and includes the uncertainty from both terrestrial and marine samples (Reimer and Reimer, 2017). Our two samples that are not paired with a terrestrial sample (22GROm-1 and 9) are similar in age to one of our paired samples (22GROm-4 and 6), and so we apply this ΔR with Marine20 in Calib8.1 to calibrate the marine bivalve ages (Reimer and Reimer, 2017; Heaton et al., 2020; Table 2). We speculate that an embayment with local and variable freshwater input could lead to variable ΔR through time and differences with ΔR from elsewhere, so we assume our local ΔR constraints are more accurate than using the ΔR reported for the Canadian Arctic Archipelago (Pieńkowski et al., 2023).

Supplementary Tables 1–3 supply the information to recalculate our radiocarbon ages as well as the compiled regional ages shown in Figures 1, 2, 5, and 6 and Table 2. Regional data are recalculated with IntCal20 and Marine 20 in Calib8.1 (Heaton et al., 2020; Reimer et al., 2020) with the ΔR of 188 ± 91 ^{14}C yr BP, as suggested for northwestern Canadian Arctic Archipelago (Pieńkowski et al., 2023). We calculate a local ΔR and apply this to the radiocarbon ages for the Mason (2010) Early Holocene marine bivalves, because they lived in similar space (<20 km away) and time (~9000–8000 yr BP) as our ΔR reconstructions. Using the Pieńkowski et al. (2023) ΔR value instead would shift ages 400 years younger at most and does not change our results or interpretations (Supplementary Table 5). We depict the most likely relative sea-level history with a line from the marine limit, above the limiting data, through the SLIPs, and to the present. We compare our data with regional sea-level histories illustrated in similar fashion, except for sea-level histories from Glueder et al. (2022), which include an error-in-variables modeling approach to predict the sea-level history (Cahill et al., 2015).

Results

The terraces we sampled from are composed of silty and sandy foreset beds containing both articulated marine bivalves and terrestrial macrofossils, which are overlain by horizontal gravelly topset beds with occasional boulders on terrace surfaces (Fig. 4). In some places, terrace surfaces contain storm beach berms. The presence of steeply dipping foreset and subhorizontal topset beds are characteristic of Gilbert-style deltas where past sea-level elevation is interpreted to be at the foreset/topset contact (Gilbert, 1890). We found this contact to be within 1 to 2 m of terrace surfaces.

Tables 1 and 2 and Figure 5 show the elevation–age relationship of the marine terraces we sampled. Terrace 1, the highest terrace, has a surface elevation of 85 ± 4 m asl. We were unable to expose sediments here and did not find material for radiocarbon dating. In Terrace 2 (surface at 66 ± 4 m asl), we collected an articulated *Hiatella arctica* shell from foreset beds that dates to 8900–8160 cal yr BP. We sampled an articulated *Astarte borealis* shell and *Calligeron* sp. moss from the foreset beds of Terrace 3 (52 ± 4 m asl); the *Calligeron* moss dates to 9010–8650 cal yr BP. From Terrace 4 (45 ± 4 m asl), we sampled an unidentifiable shell fragment from a shallow pit (<1 m) that we dug into the terrace surface that dates to 7880–7400 cal yr BP; there were no natural exposures in this terrace level. Terrace 5 is at 39 ± 4 m asl, where a 1.5-m-thick cobble-rich topset bed overlies foreset beds; the edge of this terrace has an ~1-m-high beach ridge. We sampled an articulated *Mya truncata* bivalve and *Calligeron* sp. moss from the foreset beds ~1 m beneath the topset beds; the *Calligeron* moss dates to 7970–7790 cal yr BP. Finally, Terrace 6 is at 10 ± 4 m asl, where a <1-m-thick topset bed caps the terrace. We sampled an articulated *Mya truncata* bivalve and *Salix* sp. stem from the foreset beds; the *Salix* stem dates to 5320–5060 cal yr BP. The ΔR from the 52 ± 4, 39 ± 4, and 10 ± 4 m asl terrace sample pair is −123 ± 135, 29 ± 104, and −35 ± 125 ^{14}C yr BP, respectively.

https://doi.org/10.1017/qua.2025.10049 Published online by Cambridge University Press

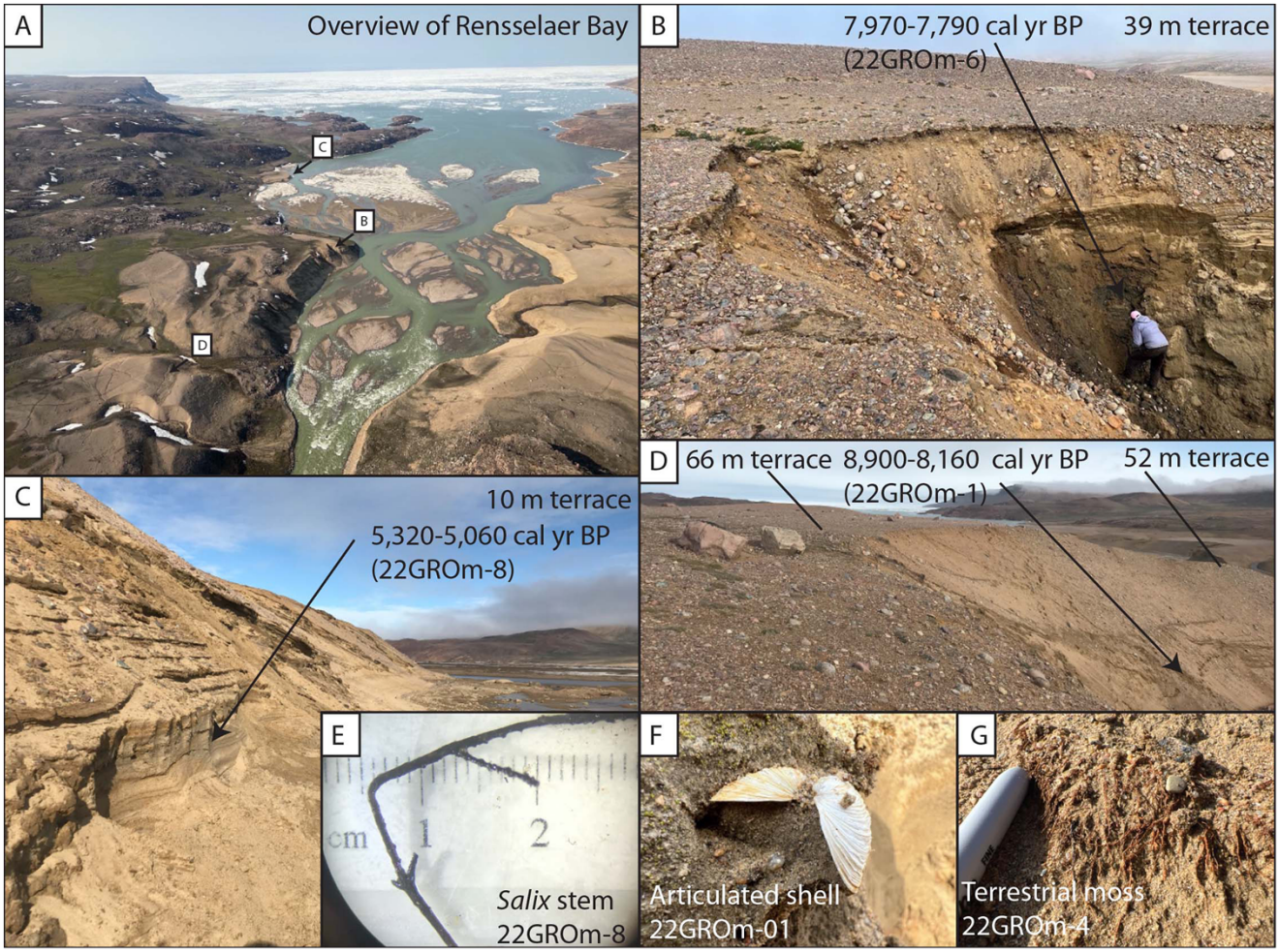

Figure 4. Field images of raised terraces and example radiocarbon samples. (**A**) Overview of Rensselaer Bay from above showing the modern river and delta (center) and Terraces 2–6 (left of river). (**B**) Terrace 5 at 39 ± 4 m asl. Person for scale at sampling location—foreset beds are shown in cross section, and topset gravel beds covered in colluvium. (**C**) Terrace 6 at 10 ± 4 m asl. This shows the dipping foreset beds and the modern river on the right. (**D**) Terraces 2 and 3 at 66 ± 4 and 52 ± 4 m asl, respectively. Some foreset beds can be seen behind the footprints. (**E**) *Salix* stem from Terrace 6 (sample 22GROm-08; 5320-5060 cal yr BP). (**F**) Articulated marine bivalve within the foreset beds of Terrace 2 (sample 22GROm-01; 8900–8160 cal yr BP). (**G**) Terrestrial *Calligeron* sp. mosses protruding from the foreset beds in Terrace 3 (sample 22GROm-04; 9010–8650 cal yr BP).

Table 1. Terrace elevation data.

Terrace name	Landform	Terrace elevation ±4 (m)	^{14}C sample elevation ±4 (m)	Topset bed thickness (m)	Past sea-level elevation ±4 (m)	Sea-level relationship to ^{14}C sample[a]	Associated age
Terrace 1	Terrace	85.0	No sample	Not recorded	85.0	Minimum	>9260–8490
Terrace 2	Strath (?) terrace	66.0	62.0	Not found	66.0	Minimum	>8900–8160
Terrace 3	Strath (?) terrace	52.0	51.0	Not recorded	52.0	Minimum	>9010–8650
Terrace 4	Strath (?) terrace	45.0	4650	Not recorded	45.0	Minimum	7880-7400 (Not used)
Terrace 5	Raised marine delta	39.0	36.5	1.5	37.5	SLIP	7970–7790
Terrace 6	Raised marine delta	10.0	7.0	1.0	9.0	SLIP	5320–5060

[a]SLIP, sea level index point.

Interpretation

Because we found no marine bivalves associated with Terrace 1 at 85 ± 4 m asl and there was no natural exposure of this terrace, we do not know if this terrace is a remnant of a fluvial terrace that graded to a marine limit or if this terrace is a marine delta formed with the marine limit. We interpret the sea-level height associated

https://doi.org/10.1017/qua.2025.10049 Published online by Cambridge University Press

https://doi.org/10.1017/qua.2025.10049 Published online by Cambridge University Press

Table 2. Radiocarbon information listed by elevation[a].

Lab code	Sample name	Latitude (°N)	Longitude (°W)	Sea-level elevation ±4 (m)	Material dated	Mass (mg)	$\delta^{13}C$‰	Fraction modern	Fraction modern error	^{14}C (BP)	^{14}C error (BP)	ΔR (^{14}C yr)	2σ age range (cal yr BP)		
This study															
182322	22GROm−1	78.578	70.710	>66.0	*Hiatella arctica*	717.4	0.1	0.3676	0.0011	8040	25	−123±135	8900	8160	100%
182323	22GROm−3	78.578	70.708	>52.0	*Astarte borealis*	91.7	−0.7	0.3537	0.0011	8350	25	−123±135	9260	8490	100%
182319	22GROm−4	78.578	70.708	>52.0	*Calligeron* sp.	4.9	−26.0	0.3689	0.0022	8010	50	NA	9010	8700	97%
182324	22GROm−9	78.581	70.712	>45.0	Bivalve fragment	158.4	1.0	0.3997	0.0012	7370	25	29±104	7880	7400	100%
182325	22GROm−10	78.584	70.714	37.5	*Mya truncata*	323.4	0.9	0.3864	0.0011	7640	25	29±104	8150	7650	100%
182320	22GROm−6	78.584	70.714	37.5	*Calligeron* sp.	4.2	−24.4	0.4153	0.0021	7060	40	NA	7970	7790	100%
182326	22GROm−7	78.588	70.740	9.0	*Mya truncata*	33.3	1.4	0.5342	0.0016	5040	25	−35±125	5530	4860	100%
182321	22GROm−8	78.588	70.740	9.0	*Salix* sp.	9.6	−26.7	0.5675	0.0015	4550	20	NA	5320	5060	100%
Mason (2010)															
AA−83054	08−04−01	78.590	71.570	52.0	Marine bivalve	NA	1.8	NA	NA	7992	50	−123±135	8070	8840	100%
AA−83057	08−07−01	78.590	71.570	31.0	Marine bivalve	NA	2.4	NA	NA	7717	49	29±104	7690	8240	100%
AA−83060	08−10−03a	78.590	71.570	62.0	Marine bivalve	NA	2.2	NA	NA	8032	51	−123±135	8130	8910	100%
AA−83056	08−13−01	78.590	−71.570	25.0	Tellinidae bivalve	NA	1.7	NA	NA	7924	51	−123±135	7990	8720	100%
AA−83061	08−17−01	78.590	71.570	31.0	Marine bivalves (n≥25)	NA	2.4	NA	NA	7814	50	29±104	7810	8340	100%

(*Continued*)

https://doi.org/10.1017/qua.2025.10049 Published online by Cambridge University Press

Table 2. (*Continued.*)

Lab code	Sample name	Latitude (°N)	Longitude (°W)	Sea-level elevation ±4 (m)	Material dated	Mass (mg)	$\delta^{13}C$‰	Fraction modern	Fraction modern error	^{14}C (BP)	^{14}C error (BP)	ΔR (^{14}C yr)	2σ age range (cal yr BP)		
AA83639	NA	78.590	71.570	5.0	Caribou/muskox bone	NA	−21.3	NA	NA	726	42	NA	565	730	100%
AA83640	NA	78.590	71.570	5.0	Caribou/muskox bone	NA	−21.6	NA	NA	828	42	NA	670	795	99%
AA83637	NA	78.590	71.570	3.0	Caribou bone	NA	−19.6	NA	NA	603	42	NA	540	655	100%
AA83638	NA	78.590	71.570	3.0	Caribou bone	NA	−18.9	NA	NA	613	42	NA	540	660	100%
AA85146	NA	78.590	71.570	3.0	Caribou bone	NA	−19.2	NA	NA	606	58	NA	530	665	100%
AA85147	NA	78.590	71.570	3.0	Muskox bone	NA	−18.9	NA	NA	672	59	NA	545	690	99%
AA85148	NA	78.590	71.570	3.0	Caribou bone	NA	−19.8	NA	NA	655	58	NA	545	680	100%
AA85149	NA	78.590	71.570	3.0	Caribou bone	NA	−19.5	NA	NA	659	58	NA	545	680	100%
AA85150	NA	78.590	71.570	3.0	Caribou bone	NA	−19.8	NA	NA	714	59	NA	555	730	100%
AA85151	NA	78.590	71.570	3.0	Caribou bone	NA	−18.9	NA	NA	605	59	NA	530	665	100%
AA85151a	NA	78.590	71.570	4.0	Caribou bone	NA	−17.5	NA	NA	658	53	NA	550	675	100%

[a]NA, not applicable/available.

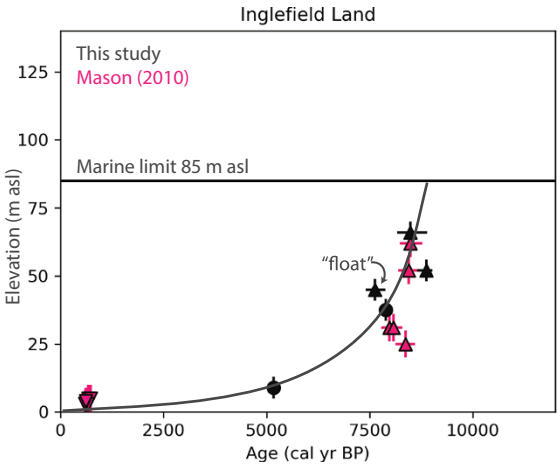

Figure 5. The radiocarbon ages from Inglefield Land plotted against elevation. The marine limit is the solid black line at 85 m. New minimum-limiting constraints are shown by upward-facing black triangles. New sea level index points (SLIPs) are shown by black circles. Relative sea-level history drawn through the SLIPs and estimated from 5000 cal yr BP to the present. Mason (2010) data are shown in pink, with minimum limits as upward triangles and maximum limits as downward triangles.

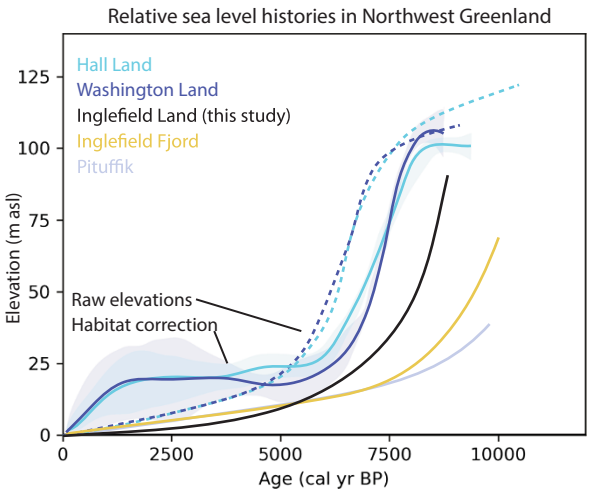

Figure 6. Combined relative sea level histories from Pituffik to Hall Land. Colors are the same as in Figures 1 and 2. The solid teal curve with uncertainty is the relative sea level history proposed from Glueder et al. (2022) for Hall Land. The solid purple curve with uncertainty is the same as the teal curve but for Washington Land. The dashed teal and purple curves are sea-level histories drawn for Hall Land and Washington Land when data from Kelly and Bennike (1992), England (1985), Bennike (2002), and Glueder et al. (2022) are all drawn as minimum-limiting data (i.e., the raw elevation from Glueder et al. [2022]). The dashed lines are the same as the raw elevation plots of Hall Land and Washington Land from Figure 2. The black curve is from this study. The yellow curve is estimated from Inglefield Fjord (Fredskild, 1985). The light purple curve is estimated from Pituffik (Funder, 1990).

with this terrace to have been 85 ± 4 m asl or lower. The oldest age from our analysis, from Terrace 3, is the closest constraint on the marine limit, so we assign 9010–8650 cal yr BP as our closest minimum-limiting constraint on both deglaciation and the marine limit.

Nichols (1969) noted that some terraces in Rensselaer Valley have foreset beds that extend to the top of the terrace. They explained this observation as fluvial erosion of previously

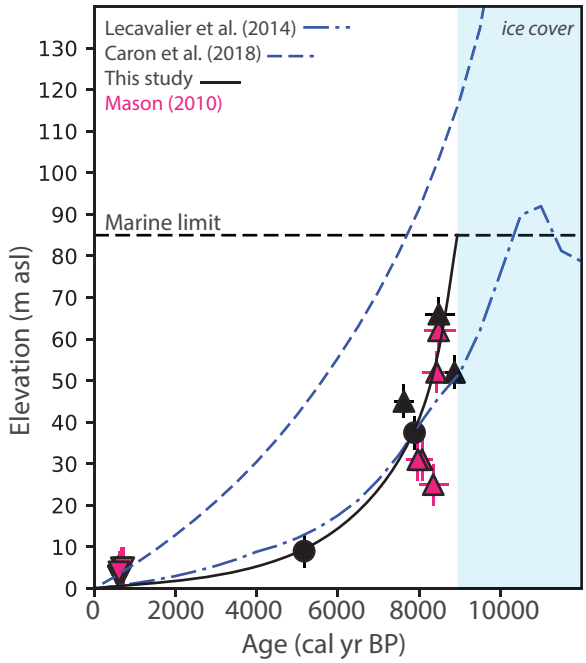

Figure 7. Data-model comparison between relative sea level reconstruction in this study and glacial isostatic adjustment model predictions of relative sea level for our study site. The blue dash-dot curve is from Lecavalier et al. (2014). The blue dashed curve is from Caron et al. (2018). Our reconstruction is shown with black triangles for limiting data and black circles for sea level index points (SLIPs). Data from Mason (2010) are shown as upward and downward pink triangles for minimum- and maximum-limiting constraints, respectively. The blue shaded box indicates when Rensselaer Valley was covered with ice (until ~9 ka).

deposited (higher-elevation) marine deltas and removal of the topset bed and some amount of the foreset beds. If this were the case, samples from such foreset beds would be unrelated to the current (strath) terrace surface elevation and the age associated with a higher relative sea level. However, if the upper terrace sediments were indeed planed off from fluvial erosion, subhorizontal fluvial deposits associated with river deposition (which would appear as topset beds) might be expected, but these were not observed. In any case, we find it safest to interpret radiocarbon ages from terraces lacking topset beds as underestimating sea-level elevation at that time and use them as minimum constraints.

We found that Terrace 2 at 66 ± 4 m asl lacks topset beds and has foreset beds that extend to the surface; therefore, we use this sample as a minimum constraint. The terrestrial sample from Terrace 3 (52 ± 4 m asl; 9010–8650 cal yr BP) is the same age within uncertainty as the marine bivalve from Terrace 2 (8900–8160 cal yr BP). It is possible that the surface at 52 ± 4 m may be a strath terrace cut into older marine delta sediments. Because we are unsure, we consider this sample a minimum constraint on sea level as well and plot Terraces 2 and 3 in Figure 5 by their terrace elevation (Table 1). However, because it appears sea level was falling rapidly at this time, these ages are likely to be very close minimums on sea-level elevation.

The ages from Terraces 4 and 5 (45 ± 4 m asl; 7880–7400 cal yr BP; and 39 ± 4 m asl; 7970–7790 cal yr BP) overlap within uncertainty, but the Terrace 4 sample is likely out of stratigraphic order. The Terrace 4 sample is a single fragment found in a shallow pit and may not be in situ, so we believe it has a reasonable chance of upslope reworking from birds or wind. Therefore, we do not use the sample from Terrace 4 in our relative sea-level analysis and label the sample "float" in Figure 5.

https://doi.org/10.1017/qua.2025.10049 Published online by Cambridge University Press

We have confidence that the Terrace 5 radiocarbon sample (39 ± 4 m asl; 7970–7790 cal yr BP) is a SLIP, because there is an identifiable topset/foreset contact in the terrace and a beach berm preserved on the outer edge of the terrace surface. Finally, Terrace 6 has a topset/foreset contact, so we also interpret this radiocarbon age and elevation as a SLIP (10 ± 4 m asl; 5320–5060 cal yr BP). In Figure 5, these data points are plotted as SLIPs with the elevation of the topset/foreset contact.

Discussion

The pattern of Holocene sea-level change

The timing of deglaciation in Inglefield Land agrees with prior reconstructions of the unzipping of the two coalesced ice sheets. Our oldest terrestrial radiocarbon date of 9010–8650 cal yr BP lies between the oldest dates from Inglefield Fjord (9760–8910 cal yr BP) and southwest Washington Land (7920–7450 cal yr BP; Fredskild, 1985; Bennike, 2002). The date also agrees with sediment cores from Kane Basin in southern Nares Strait, ~100 km due north of our study site, that constrain deglaciation to ~8900–8560 cal yr BP (Georgiadis et al., 2018) and peat from marine terraces in Rensselaer Valley of 9130–8180 cal yr BP (Nichols, 1969).

In Rensselaer Valley, sea level fell rapidly from the marine limit to our first SLIP from 9010–8650 to 7970–7790 cal yr BP at a rate of 49 m/ka. The rate of sea-level fall slowed to 11 m/ka between our two SLIPs at 7970–7790 and 5320–5060 cal yr BP. After 5320–5060 cal yr BP, our best estimate of steady sea-level fall to the present results in a decrease to 2 m/ka. Our data indicate thick last glacial maximum ice over our study area; sea level fell rapidly between the marine limit and the first SLIP ~8000 cal yr BP, showing that the land was rebounding quickly upon deglaciation.

There is conflicting evidence from Mason (2010) and Nichols (1969) about evidence of standstills in the geomorphology of the beach ridges at Rensselaer Bay. Mason (2010) described the beaches in Cape Grinnell (Fig. 1) and interpreted a sea-level standstill at 20 m asl and a short-lived transgression at 5 m asl. If we use our relative sea level reconstruction between 8000 and 5000 cal yr BP (from SLIPs), such a 20 m standstill would have occurred ~6200 cal yr BP. Such a sea-level oscillation at 5 m asl would have occurred ~3700 cal yr BP. Sea level had five more meters to fall between this standstill and present sea level between 3700 cal yr BP and the present. If this transgression did last multiple millennia, sea level had to fall five more meters to intersect modern sea level, and this would cause rapid sea-level fall during the coldest interval in north Greenland, and challenge the regional ice histories (e.g., of Ruesch et al., 2018). The possibility of a Late Holocene standstill is also challenged by the geomorphology reported by Nichols (1969), who interpreted steady sea-level fall from the marine limit to present from beach ridges 4 km from our study site. Continuous sea-level fall shown by Nichols (1969) does not rule out a J-shape sea-level curve, in which sea level falls below present and rises the equivalent to present sea level (Long et al., 2009). The beach ridges closest to the ocean could be, for example, ~4000–3000 years old and sea level could have risen from a low point to the modern elevation after ~2000–1000 years ago. Neither of these publications nor our own, however, have age control after 5000 cal yr BP. Thus, more attention to raised terraces between 10 m asl and present sea level would help reconcile the relative sea-level history in the Middle and Late Holocene.

Figure 6 shows that the sea-level history of Inglefield Land captures the transition between the style of emergence in southern and northern Nares Strait. Supplementary Table 4 supplies information to calculate regional rates of sea level change. Even though there are few data to constrain the curves drawn in Figure 6 from Inglefield Fjord and Pituffik, the general trend of the decreasing marine limits from Pituffik to Hall Land shows the influence of the increased ice load in the center of Nares Strait. While Washington and Hall Land have higher marine limits, constraints show a slow rate (5 m/ka and 3 m/ka, respectively) of emergence after deglaciation that leads to lower rates overall. This delay in the emergence rate may be from slower ice retreat when those sites were initially deglaciated. Washington and Hall Land have their highest rates of sea level fall between ~7.6 and 5 cal ka BP (30 m/ka) and ~8.4 and 5.8 cal ka BP (34 m/ka). Inglefield Fjord had the highest rate of emergence during the same time as Inglefield Land, with a rate of 30 m/ka between ~9.4 and 7.6 cal ka BP. Finally, Pituffik has the lowest rate of emergence of 6 m/ka between ~10.5 and 7 cal ka BP, also during the same time as Inglefield Fjord and Inglefield Land. This pattern is consistent with increasing ice loading and decreasing deglaciation age toward the middle of Nares Strait.

Figure 6 shows the difference between the sea-level histories for Hall Land and Washington Land with and without the habitat correction employed by Glueder et al. (2022). The habitat-corrected sea-level data, which indicate a sea-level standstill from 6 to 2 ka, appear anomalous in the context of other records (solid teal and purple lines in Fig. 6). However, if the shell data are instead considered raw (using collection elevation instead of adjusted elevation) and hence are relative sea level minimums, the relative sea level histories are highly compatible (dashed teal and purple lines in Fig. 6). Additionally, because the habitat-corrected sea-level history is explained by an anomalous ice history compared with the rest of Greenland, we find this to be an added reason to favor the relative sea level curves based on the raw shell data.

To investigate our reconstruction further, we compare our sea-level curve with model predictions from a regional glacial isostatic adjustment model (Huy3; Lecavalier et al., 2014) and a global glacial isostatic adjustment model (Caron et al., 2018) (Fig. 7). We find that Huy3 model output has an earlier deglaciation timing than our data support, leading to a 92 m asl marine limit at ~11,000 cal yr BP. We measured an 85 ± 4 m asl marine limit that dates to ~9000 cal yr BP—a difference of only 4 m, within the uncertainty of our measurement. The early simulated deglaciation leads to sea level lowering earlier than in our reconstruction. If simulated deglaciation occurred 2000 years, the model would likely match our sea-level reconstruction even more closely. The Lecavalier et al. (2014) model matches our 8000 and 5000 cal yr BP SLIPs. This reasonably good data-model fit from deglaciation to 5000 cal yr BP supports our interpolation between 5000 and the present despite the lack of data constraints in this interval. The Caron et al. (2018) model simulates deglaciation even earlier than Huy3 (12,500 years ago), which explains their 253 m asl marine limit. This model also predicts steady sea-level fall from deglaciation to the present without a standstill or a J-shape. Thus, both the available modeling and the trajectory of our data support a smoothly declining sea-level height between 5000 cal yr BP and the present.

These modeled glacial isostatic adjustment predictions of steady sea-level fall to the present likely arise from the fact that neither considers a change in the ice margin from 7 ka to the present (Lecavalier et al., 2014; Caron et al., 2018). We know from reworked bivalves in Humbolt Glacier Little Ice Age moraines that the ice sheet was somewhere behind its present margin during the Middle–Late Holocene (Søndergaard et al., 2020). The Middle–Late Holocene ice growth may have impacted the sea-level

https://doi.org/10.1017/qua.2025.10049 Published online by Cambridge University Press

history if the scale of loading was large enough to influence the solid Earth. Glueder et al. (2022) showed there needed to be a thinner lithosphere and less viscous mantle than that originally proposed for Greenland (Lecavalier et al., 2014) to obtain their derived standstill in sea-level history. This indicates the solid Earth in northwest Greenland, with the optimally fit Earth parameters, may not be sensitive to smaller-scale ice growth-and-retreat cycles.

Conclusions

This new relative sea level curve from Inglefield Land supplements the available sea-level histories along Nares Strait, northwest Greenland, with new limiting and SLIP data. Our results show that the coast of Inglefield Land deglaciated by 9010–8650 cal yr BP, and sea level fell rapidly at a rate of 49 m/ka until 7970–7790 cal yr BP. Emergence decreased first to 11 m/ka until 5320–5060 before likely decreasing to 2 m/ka through to the present. This new sea-level history captures the transition from the style of emergence at either end of the Nares Strait: from Pituffik to Hall Land, the rate of emergence generally increases, while the period of fastest emergence is younger. This reconstruction estimates steady sea-level fall from 5000 years ago to the present, which is supported by glacial isostatic adjustment model predictions. This history agrees with the pattern of sea-level fall after ∼5000 cal yr BP when using the raw (noncorrected) elevations from Glueder et al. (2022). Future work should investigate the post–5000 year history to fully determine the evidence for standstill/J-shape and the implications for the ice history; additional SLIPs from the abundant marine deltas in other river valleys in Inglefield Land would be most useful. These data can be used to benchmark ice-sheet and glacial isostatic adjustment models in an area with a high degree of spatial heterogeneity in sea-level history.

Supplementary material. The supplementary material for this article can be found at https://doi.org/10.1017/qua.2025.10049.

Acknowledgments. We thank Caleb Walcott-George and Joerg Schaefer for help and good company in the field. Thanks to the staff at Battelle, U.S. National Science Foundation, and the U.S. Air Mobility Command for logistical and field support. Thanks to AirGreenland for helicopter support. Much gratitude to Ole Bennike for helping with macrofossil identification. Thanks to Glenn Milne and Lambert Caron for providing glacial isostatic adjustment model output. Geospatial support for this work was provided by the Polar Geospatial Center under U.S. National Science Foundation–Office of Polar Programs awards 1043681, 1559691, and 2129685. Digital elevation models (DEMs) provided by the Polar Geospatial Center under NSF-OPP awards 1043681, 1559691, 1542736, 1810976, and 2129685. This work was funded by the U.S. National Science Foundation grant no. 2106971. Finally, we thank two anonymous reviewers and associate editor T. Lowell for detailed reviews that improved this article.

Competing Interests. The authors declare no competing interests.

References

Antwerpen, R., Austermann, J., Young, N., Porter, D., Lewright, L., Latychev, K., 2024. Holocene southwest Greenland ice sheet behavior constrained by sea-level modeling. *Quaternary Science Reviews* **328**, 108553.

Axford, Y., de Vernal, A., Osterberg, E.C., 2021. Past warmth and its impacts during the Holocene thermal maximum in Greenland. *Annual Review of Earth and Planetary Sciences* **49**, 279–307.

Axford, Y., Lasher, G.E., Kelly, M.A., Osterberg, E.C., Landis, J., Schellinger, G.C., Pfeiffer, A., Thompson, E., Francis, D.R., 2019. Holocene temperature history of northwest Greenland—with new ice cap constraints and chironomid assemblages from Deltasø. *Quaternary Science Reviews* **215**, 160–172.

Batchelor, C.L., Krawczyk, D.W., O'Brien, E., Mulder, J., 2024. Shelf-break glaciation and an extensive ice shelf beyond northwest Greenland at the Last Glacial Maximum. *Marine Geology* **476**, 107375.

Bennike, O., 2002. Late Quaternary history of Washington Land, North Greenland. *Boreas* **31**, 260–272.

Blake, W.J., 1992. Holocene emergence at Cape Herschel, east-central Ellesmere Island, Arctic Canada: implications for ice sheet configuration. *Canadian Journal of Earth Sciences* **29**, 1958–1980.

Blake, W.J., Boucherle, M.M., Fredskild, B., Janssens, J.A., Smol, J., 1992. The geomorphological settings, glacial history and Holocene development of "Kap Inglefield Sø", Inglefield Land, North-West Greenland. *Meddelelser om Grønland. Geoscience* **27**, 1–42.

Briner, J.P., Cuzzone, J.K., Badgeley, J.A., Young, N.E., Steig, E.J., Morlighem, M., Schlegel, N.J., *et al.*, 2020. Rate of mass loss from the Greenland Ice Sheet will exceed Holocene values this century. *Nature* **586**, 70–74.

Briner, J.P., McKay, N.P., Axford, Y., Bennike, O., Bradley, R.S., de Vernal, A., Fisher, D., *et al.*, 2016. Holocene climate change in Arctic Canada and Greenland. *Quaternary Science Reviews* **147**, 340–364.

Cahill, N., Kemp, A.C., Horton, B.P., Parnell, A.C., 2015. Modeling sea-level change using errors-in-variables integrated Gaussian processes. *Annals of Applied Statistics* **9**, 547–571.

Caron, L., Ivins, E.R., Larour, E., Adhikari, S., Nilsson, J., Blewitt, G., 2018. GIA model statistics for GRACE hydrology, cryosphere, and ocean science. *Geophysical Research Letters* **45**, 2203–2212.

Couette, P.-O., Lajeunesse, P., Ghienne, J.-F., Dorschel, B., Gebhardt, C., Hebbeln, D., Brouard, E., 2022. Evidence for an extensive ice shelf in northern Baffin Bay during the Last Glacial Maximum. *Communications Earth & Environment* **3**, 225.

Edwards, T.L., Nowicki, S., Marzeion, B., Hock, R., Goelzer, H., Seroussi, H., Jourdain, N.C., *et al.*, 2021. Projected land ice contributions to twenty-first-century sea level rise. Nature **593**, 74–82.

Elder, K.L., Roberts, M.L., Walther, T., Xu, L., 2019. Single step production of graphite from organic samples for radiocarbon measurements. *Radiocarbon* **61**, 1843–1854.

England, J., 1985. The late Quaternary history of Hall Land, northwest Greenland. *Canadian Journal of Earth Sciences* **22**, 1394–1408.

England, J., 1999. Coalescent Greenland and Innuitian ice during the Last Glacial Maximum: revising the Quaternary of the Canadian High Arctic. *Quaternary Science Reviews* **18**, 421–456.

Fredskild, B., 1985. The Holocene vegetational development of Tugtuligssuaq and Qeqertat, Northwest Greenland. *Meddelelser om Grønland. Geoscience* **22**, 1–4.

Funder, S., 1990. Late Quaternary stratigraphy and glaciology in the Thule area, northwest Greenland. Museum Tusculanum Press. https://doi.org/10.7146/moggeosci.v22i.140140.

Georgiadis, E., Giraudeau, J., Martinez, P., Lajeunesse, P., St-Onge, G., Schmidt, S., Massé, G., 2018. Deglacial to postglacial history of Nares Strait, Northwest Greenland: a marine perspective from Kane Basin. *Climate of the Past* **14**, 1991–2010.

Gilbert, G.K., 1890. *Lake Bonneville*. Monograph 1. U.S. Geological Survey, Washington, DC, p. 438. https://doi.org/10.3133/m1.

Glueder, A., Mix, A.C., Milne, G.A., Reilly, B.T., Clark, J., Jakobsson, M., Mayer, L., Fallon, S.J., Southon, J., Padman, J., 2022. Calibrated relative sea levels constrain isostatic adjustment and ice history in northwest Greenland. *Quaternary Science Reviews* **293**, 107700.

Goelzer, H., Nowicki, S., Payne, A., Larour, E., Seroussi, H., Lipscomb, W.H., Gregory, J., *et al.*, 2020. The future sea-level contribution of the Greenland ice sheet: a multi-model ensemble study of ISMIP6. *The Cryosphere* **14**, 3071–3096.

Gowan, E.J., 2023. Paleo sea-level indicators and proxies from Greenland in the GAPSLIP database and comparison with modelled sea level from the PaleoMIST ice-sheet reconstruction. *GEUS Bulletin* 53. https://doi.org/10.34194/geusb.v53.8355.

Hall, B.L., Baroni, C., Denton, G.H., 2010. Relative sea-level changes, Schuchert Dal, East Greenland, with implications for ice extent in late-glacial and Holocene times. *Quaternary Science Reviews* **29**, 3370–3378.

Heaton, T.J., Köhler, P., Butzin, M., Bard, E., Reimer, R.W., Austin, W.E., Ramsey, C.B., Grootes, P.M., Hughen, K.A., Kromer, B., 2020. Marine20—the marine radiocarbon age calibration curve (0–55,000 cal BP). *Radiocarbon* **62**, 779–820.

IPCC, 2019. Summary for policymakers. In: Pörtner, H.-O., Roberts, D.C., Masson-Delmotte, V., Zhai, P., Tignor, M., Poloczanska, E., Mintenbeck, K., ***et al.*** (Eds.), *IPCC Special Report on the Ocean and Cryosphere in a Changing Climate*. Cambridge University Press, Cambridge, pp. 3–35.

Kelly, M., Bennike, O., 1992. Quaternary geology of western and central North Greenland. *Rapport Grønlands Geologiske Undersøgelse* **153**, 1–34.

Kelly, M., Funder, S., Houmark-nielsen, M., Knudsen, K.L., Kronborg, C., Landvik, J., Sorby, L., 1999. Quaternary glacial and marine environmental history of northwest Greenland: a review and reappraisal. *Quaternary Science Reviews* **18**, 373–392.

Kjær, K.H., Bjørk, A.A., Kjeldsen, K.K., Hansen, E.S., Andresen, C.S., Siggaard-Andersen, M.-L., Khan, S.A., *et al.*, 2022. Glacier response to the Little Ice Age during the Neoglacial cooling in Greenland. *Earth-Science Reviews* **227**, 103984.

Lasher, G.E., Axford, Y., McFarlin, J.M., Kelly, M.A., Osterberg, E.C., Berkelhammer, M.B., 2017. Holocene temperatures and isotopes of precipitation in Northwest Greenland recorded in lacustrine organic materials. *Quaternary Science Reviews* **170**, 45–55.

Lecavalier, B.S., Fisher, D.A., Milne, G.A., Vinther, B.M., Tarasov, L., Huybrechts, P., Lacelle, D., *et al.*, 2017. High Arctic Holocene temperature record from the Agassiz ice cap and Greenland ice sheet evolution. *Proceedings of the National Academy of Sciences USA* **114**, 5952–5957.

Lecavalier, B.S., Milne, G.A., Simpson, M.J.R., Wake, L., Huybrechts, P., Tarasov, L., Kjeldsen, K.K., *et al.*, 2014. A model of Greenland ice sheet deglaciation constrained by observations of relative sea level and ice extent. *Quaternary Science Reviews* **102**, 54–84.

Leger, T.P.M., Clark, C.D., Huynh, C., Jones, S., Ely, J.C., Bradley, S.L., Diemont, C., Hughes, A.L.C., 2024. A Greenland-wide empirical reconstruction of paleo ice sheet retreat informed by ice extent markers: PaleoGrIS version 1.0. *Climate of the Past* **20**, 701–755.

Long, A.J., Woodroffe, S.A., Dawson, S., Roberts, D.H., Bryant, C.L., 2009. Late Holocene relative sea level rise and the Neoglacial history of the Greenland ice sheet. *Journal of Quaternary Science* **24**, 345–359.

Long, A.J., Woodroffe, S.A., Roberts, D.H., Dawson, S., 2011. Isolation basins, sea-level changes and the Holocene history of the Greenland Ice Sheet. *Quaternary Science Reviews* **30**, 3748–3768.

Mason, O.K., 2010. Beach ridge geomorphology at Cape Grinnell, northern Greenland: a less icy Arctic in the mid-Holocene. *Geografisk Tidsskrift-Danish Journal of Geography* **110**, 337–355.

Morlighem, M., Williams, C.N., Rignot, E., An, L., Arndt, J.E., Bamber, J.L., Catania, G., *et al.*, 2017. BedMachine v3: complete bed topography and ocean bathymetry mapping of Greenland from multibeam echo sounding combined with mass conservation. *Geophysical Research Letters* **44**, 11051–11061.

Morlighem, M., Williams, C.N., Rignot, E., An, L., Arndt, J.E., Bamber, J.L., Catania, G., *et al.*, 2021. IceBridge BedMachine Greenland, Version 4. NASA National Snow and Ice Data Center Distributed Active Archive Center. https://doi.org/10.5067/VLJ5YXKCNGXO.

Nichols, R.L., 1969. Geomorphology of Inglefield Land, North Greenland. *Meddelelser om Grønland* **188**(1).

Pearson, A., McNichol, A.P., Schneider, R.J., Von Reden, K.F., Zheng, Y., 1997. Microscale AMS ^{14}C Measurement at NOSAMS. *Radiocarbon* **40**, 61–75.

Pieńkowski, A.J., Coulthard, R.D., Furze, M.F.A., 2023. Revised marine reservoir offset (ΔR) values for molluscs and marine mammals from Arctic North America. *Boreas* **52**, 145–167.

Porter, C., Howat, I., Noh, M.-J., Husby, E., Khuvis, S., Danish, E., Tomko, K., *et al.*, 2023. ArcticDEM—Mosaics, Version 4.1. Harvard Dataverse, Version 1. https://doi.org/10.7910/DVN/3VDC4W.

Reimer, P.J., Austin, W.E.N., Bard, E., Bayliss, A., Blackwell, P.G., Bronk Ramsey, C., Butzin, M., *et al.*, 2020. The IntCal20 Northern Hemisphere Radiocarbon Age Calibration Curve (0–55 cal kBP). *Radiocarbon* **62**, 725–757.

Reimer, R.W., Reimer, P.J., 2017. An online application for ΔR calculation. *Radiocarbon* **59**, 1623–1627.

Reusche, M.M., Marcott, S.A., Ceperley, E.G., Barth, A.M., Brook, E.J., Mix, A.C., Caffee, M.W., 2018. Early to Late Holocene surface exposure ages from two marine-terminating outlet glaciers in northwest Greenland. *Geophysical Research Letters* **45**, 7028–7039.

RGI Consortium, 2023. Randolph Glacier Inventory–A Dataset of Global Glacier Outlines, Version 7. NASA National Snow and Ice Data Center Distributed Active Archive Center. https://doi.org/10.5067/F6JMOVY5NAVZ.

Shah Walter, S.R., Gagnon, A.R., Roberts, M.L., McNichol, A.P., Gaylord, M.C.L., Klein, E., 2015. Ultra-small graphitization reactors for ultra-microscale ^{14}C analysis at the National Ocean Sciences Accelerator Mass Spectrometry (NOSAMS) Facility. *Radiocarbon* **57**, 109–122.

Søndergaard, A.S., Larsen, N.K., Steinemann, O., Olsen, J., Funder, S., Egholm, D.L., Kjær, K.H., 2020. Glacial history of Inglefield Land, north Greenland from combined in situ 10Be and 14C exposure dating. *Climate of the Past* **16**, 1999–2015.

Stuiver, M., Reimer, P.J., 1993. Extended ^{14}C data base and revised CALIB 3.0 ^{14}C age calibration program. *Radiocarbon* **35**, 215–230.

Vogel, J.S., Southon, J.R., Nelson, D.E., Brown, T.A., 1984. Performance of catalytically condensed carbon for use in accelerator mass spectrometry. *Nuclear Instruments and Methods in Physics Research Section B: Beam Interactions with Materials and Atoms* **5**, 289–293.

Weidick, A., 1977. A reconnaissance of Quaternary deposits in northern Greenland. *Rapport Grønlands Geologiske Undersøgelse* **85**, 21–24.

https://doi.org/10.1017/qua.2025.10049 Published online by Cambridge University Press